

MSDE

Molecular Systems Design & Engineering

Accepted Manuscript

This article can be cited before page numbers have been issued, to do this please use: Y. Nakagawa, H. L. Mizuno, Y. Ushimaru, J. Norimatsu, K. Igarashi, K. Masuda, M. Takai, Y. Anraku and H. Cabral, *Mol. Syst. Des. Eng.*, 2024, DOI: 10.1039/D4ME00105B.



This is an Accepted Manuscript, which has been through the Royal Society of Chemistry peer review process and has been accepted for publication.

Accepted Manuscripts are published online shortly after acceptance, before technical editing, formatting and proof reading. Using this free service, authors can make their results available to the community, in citable form, before we publish the edited article. We will replace this Accepted Manuscript with the edited and formatted Advance Article as soon as it is available.

You can find more information about Accepted Manuscripts in the [Information for Authors](#).

Please note that technical editing may introduce minor changes to the text and/or graphics, which may alter content. The journal's standard [Terms & Conditions](#) and the [Ethical guidelines](#) still apply. In no event shall the Royal Society of Chemistry be held responsible for any errors or omissions in this Accepted Manuscript or any consequences arising from the use of any information it contains.

Singlet oxygen ($^1\text{O}_2$) plays a crucial role in various biological processes, including cellular signaling and oxidative stress, necessitating reliable methods for its detection and quantification. However, detecting $^1\text{O}_2$ in biological systems is challenging due to its high reactivity and short lifespan. Here, we developed dually-labelled polymeric micelles (SOSG@Cy5-PIC/m) capable of detecting $^1\text{O}_2$ and reporting probe positions. These micelles are formed using oppositely charged diblock copolymers, Cy5-conjugated PEG-poly(α,β -aspartic acid) and Cy5-conjugated PEG[1]poly([5-aminopentyl]- α,β -aspartamide), which self-assemble in aqueous solution. Singlet Oxygen Sensor Green (SOSG) molecules, which fluoresce upon interaction with $^1\text{O}_2$, are integrated into the micelle core by condensation to the amines in the poly([5-aminopentyl]- α,β -aspartamide) block. The micelle core is crosslinked by forming amide bonds between the carboxylates in the poly(α,β [1]aspartic acid) segment and the amines in the poly([5-aminopentyl]- α,β -aspartamide) block, ensuring stability in biological environments. The micelles are around 30 nm and the dyes in their core are protected by a dense PEG shell. The micelles quantitatively detect $^1\text{O}_2$ in media and enable visualization of $^1\text{O}_2$ in 3D cellular spheroids under induced cellular stress. Potential applications include advancing research tools for understanding $^1\text{O}_2$, diagnostics for oxidative stress-related diseases and exploring targeted therapies, such as photodynamic therapy. Future developments may enhance sensitivity and targeting capabilities for broader biomedical applications.



COMMUNICATION

6 Dual-Labelled Polymeric Micelles for Singlet Oxygen Reporting in 7 Biological Systems

8 Yasuhiro Nakagawa^{1, 2, 3†}, Hayato Laurence Mizuno^{2, 3}, Yuta Ushimaru¹, Jumpei Norimatsu¹,
9 Kazunori Igarashi^{1, 2}, Keita Masuda¹, Madoka Takai¹, Yasutaka Anraku^{2, 3}, Horacio Cabral^{1, 2*}

10 Received 00th January 20xx,
11 Accepted 00th January 20xx

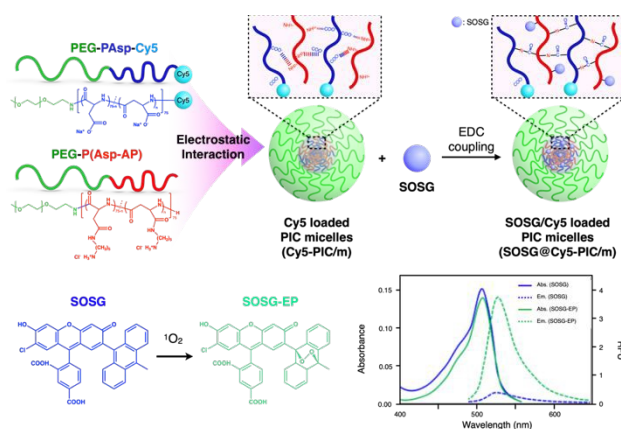
12 DOI: 10.1039/x0xx00000x

13 Visualizing singlet oxygen (¹O₂) in biological systems could greatly
14 enhance our understanding of its biological roles and offer new
15 diagnostics and therapeutics. However, ¹O₂ is unstable and highly
16 reactive, making its detection in living systems a significant
17 challenge. To address this, we have developed dually-labelled
18 polymeric micelles designed to trace both the location and levels
19 of ¹O₂.

20 Reactive oxygen species (ROS), *e.g.*, super oxide anions (O₂⁻),
21 hydrogen peroxide (H₂O₂), and ¹O₂, are important mediators in a
22 variety of biological and pathological processes [1, 2]. The ROS are
23 involved in essential biological functions, such as signalling, cell
24 metabolism, and regulation of the immune system [3]. When ROS are
25 overproduced or antioxidants are depleted, these reactive species
26 cause oxidative stress, oxidizing lipids, proteins, carbohydrates, RNA,
27 and DNA, which leads to cellular damage. Such damage is linked to
28 various diseases, including cardiovascular disease, neurodegenerative
29 disorders, and cancer [4, 5, 6, 7]. Moreover, high ROS levels can be
30 used for therapeutically damaging cancer cells [8]. In fact, a major
31 physiological mechanism to kill tumour cells is the production of ROS
32 by neutrophils and macrophages [9]. Moreover, certain anticancer
33 drugs can induce ROS production. For instance, oxaliplatin, a widely
34 used chemotherapeutic agent [10], can directly affect mitochondria,
35 inducing mitochondrial permeability transition and ROS generation
36 [11, 12]. Thus, an improved understanding of the role of ROS in
37 living systems can provide opportunities for developing innovative
38 diagnostic and therapeutic strategies.

39 Detection of ¹O₂ has been attracting much attention, as it is
40 involved in various biological phenomena by direct reaction with
41

42 biomolecules and regulation of intracellular signals [13, 14].
43 However, because ¹O₂ has a short lifetime, high reactivity, and low
44 concentration, its detection has been challenging. Several
45 approaches have been developed for the detection of ¹O₂, including
46 direct measurement of ¹O₂ phosphorescence (transition light from
47 singlet to triplet state) at 1280 nm [15], electron spin resonance
48 spectroscopy (ESR) [16], photo/chromo-sensitizers [17], and
49 fluorescent probes [18]. Despite these major efforts, *in situ*
50 observation is still limited. Challenges include low phosphorescence
51 quantum efficiency (~10⁻⁶ for aqueous systems and even smaller for
52 systems containing ¹O₂ quencher) [19], inefficient conversion of ¹O₂
53 to stable radical species for ESR [16], toxicity and cellular damage
54 from photo/chromo-sensitizers [20], and low stability and uncertain
55 distribution of fluorescent probes in tissues and cells. Thus,
56 innovative approaches are still necessary for effective ¹O₂ sensing in
57 biological systems.



58 **Figure 1.** Schematic illustration of SOSG/Cy5-labeled PIC micelles
59 (SOSG@Cy5-PIC/m). The conjugated SOSG enables the detection of ¹O₂
60 by changing its fluorescent characteristic, while the Cy5 constantly reports
61 the position of the probes in biological systems.

62 Polymeric micelles, *i.e.*, core-shell polymeric structures, have
63 demonstrated great potential for targeted therapy and diagnosis by
64 delivering a wide variety of bioactive compounds loaded in their core
65 [21]. Moreover, the shell of the polymeric micelles can protect the

66 1. Department of Bioengineering, Graduated School of Engineering, The University
67 of Tokyo, 7-3-1 Hongo, Bunkyo-ku, Tokyo, 113-8656, Japan

68 2. Innovation Center of NanoMedicine, Kawasaki Institute of Industrial Promotion,
69 3-25-14 Tonomachi, Kawasaki-ku, Kawasaki, 210-0821, Japan

70 3. Department of Materials Science and Engineering, Graduated School of Materials
71 and Chemical Technology, Tokyo Institute of Technology, 2-12-1 Ookayama,
72 Meguro-ku, Tokyo, 152-8550, Japan

73 † Y.N. has moved to Mitsui Chemicals, Inc. (Tokyo, Japan).

74 Supplementary Information available: Materials and methods. See
75 DOI: 10.1039/x0xx00000x



bioactive agents in the core from biological degradation. Thus, polymeric micelles can navigate and spatiotemporally control the function of the payloads in biological settings [22]. Polymeric micelles can be assembled in aqueous environments by controlling the interaction of the forming block copolymers, such as hydrophobicity and electrostatic interaction between the core-forming segments. Particularly, polyion complex (PIC) micelles have been prepared using poly(ethylene glycol) (PEG) based oppositely charged segments of the block copolymer pair of PEG-poly(anion) and PEG-poly(cation). These PIC micelles (PIC/m) offer substantial advantages as reporter agents, as they allow effective size control, softness, and versatile drug loading capability [23].

Here, we developed a nano-scaled reporter based on PIC/m that is capable of indicating its distribution in living systems and sensing the presence of $^1\text{O}_2$ in their surroundings. These reporters were made by mixing oppositely charged diblock copolymers, *i.e.*, Cy5-conjugated PEG-poly(α,β -aspartic acid) (PEG-PAsp) and Cy5-conjugated PEG-poly([5-aminopentyl]- α,β -aspartamide) (PEG-P(Asp-AP)), in an aqueous solution [24]. The PIC/m were also stabilised by cross-linking the core through 1-ethyl-3-(3-dimethylaminopropyl)carbodiimide (EDC) coupling to avoid micelle dissociation in biological environments. As cross-linked PIC structures are still permeable to small biomolecules [24], Singlet Oxygen Sensor Green (SOSG) molecules, which are precise reporters of $^1\text{O}_2$ [25, 26], were conjugated to the core of the micelles to provide specific sensitivity for fluorescent detection of $^1\text{O}_2$ (Figure 1) [18]. After purification to remove the unreacted SOSG and EDC, the size and polydispersity index of the dual-labelled micelles (SOSG@Cy5-PIC/m) were 31 nm and 0.08, respectively (Figure 2a). Incorporation of Cy5 and SOSG was confirmed by fluorescence spectrometry (Figure 2b), with the emission spectrum of SOSG@Cy5-PIC/m showing peaks at 540 nm that correspond to SOSG and 680 nm that relate to Cy5. These results indicate successful preparation of SOSG@Cy5-PIC/m.

The $^1\text{O}_2$ detection capacity of SOSG@Cy5-PIC/m was evaluated by using EP, which is a convenient reagent for this purpose, as it can quantitatively generate $^1\text{O}_2$ in solution by simply heating above 35°C without using light or photosensitisers. The $^1\text{O}_2$ dose-dependent fluorescence emission of SOSG@Cy5-PIC/m showed a gradual increase of the peak at 539 nm (Figure 2c), similar to the behavior observed with free SOSG. The fluorescence intensity of SOSG@Cy5-PIC/m was stronger than that of free SOSG under 1×10^{-3} M presumably due to reduced inter-SOSG energy transfer that caused quenching of free SOSG. The increase in fluorescence intensity exhibited high linearity in relation to $^1\text{O}_2$ concentration, indicating that the micelles can quantitatively detect $^1\text{O}_2$ (Figure 2d). Importantly, the Cy5 fluorescence remained unaffected by $^1\text{O}_2$ levels (Figure 2e), reinforcing its reliability as a stable marker for PIC/m concentration. This stability enables the use of Cy5 fluorescence to normalize SOSG signal, providing a robust ratiometric approach for precise quantification of $^1\text{O}_2$ in biological samples.

The time-dependent cellular uptake of SOSG@Cy5-PIC/m was examined in monolayer and spheroid cultured cells of human pancreatic adenocarcinoma (BxPC3) *in vitro*. Polymeric micelles with their size precisely controlled below 50 nm display great permeability

against tumour tissues [21]. Thus, time-dependent internalizations of SOSG@Cy5-PIC/m in both cell culture systems were observed by confocal laser scanning microscopy (CLSM) (Figures 3a-c). The internalization of the micelle in each cell was evaluated as relative fluorescent units (RFU) per cell or spheroid. The cells cultured in monolayer showed a time-dependent increase of the RFU/cells, which became saturated at 6 h incubation (Figure 3b). Spheroid cultured cells also showed a time-dependent increase of the RFU/spheroid signal. However, the fluorescence intensity in the spheroids kept increasing even after 24 h incubation (Figure 3c).

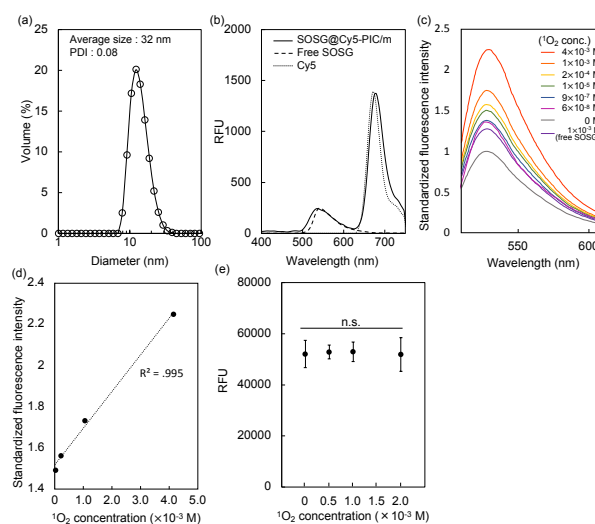


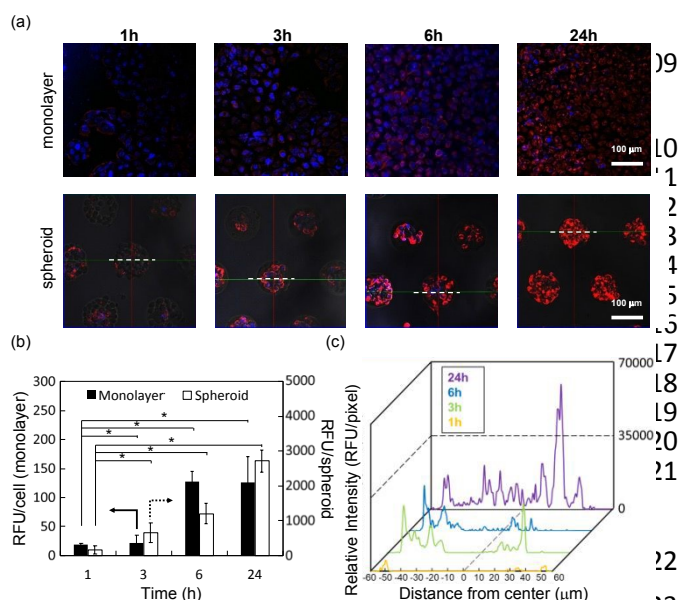
Figure 2. Characterization of the SOSG@Cy5-labeled PIC/m (SOSG@Cy5-PIC/m). (a) Size distribution of SOSG@Cy5-PIC/m determined by DLS. (b) Fluorescent spectra of SOSG@Cy5-PIC/m, SOSG, and Cy5 (Excitation (Ex) = 460 nm). (c) $^1\text{O}_2$ dose-dependent fluorescence intensity of SOSG@Cy5-PIC/m (Ex = 460 nm). (d) $^1\text{O}_2$ dose-dependent fluorescence intensity of SOSG@Cy5-PIC/m at an emission wavelength of 530 nm. (e) $^1\text{O}_2$ dose-dependent fluorescence intensity of Cy5 in PIC/m (Ex = 633 nm).

The time-dependent penetration of the SOSG@Cy5-PIC/m into the spheroid core of SOSG@Cy5-PIC/m was analysed by taking the fluorescence profile across the spheroids and summarised as histograms (Figure 3c). These histograms indicate that the SOSG@Cy5-PIC/m penetrated the spheroids time-dependently. At 1 h incubation, the micelles were barely detected in the periphery of the spheroids. Extending the incubation time to 3-6 h increased the intensity of micelles in cells located at the border of the spheroids. This also resulted in a gradual decay of the fluorescence profile toward the spheroid core. After 24 h incubation, the micelles were observed throughout the entire spheroid, including the centre of the spheroid. These results suggest that imaging the spheroid culture at 24 h is an optimal time point for detecting $^1\text{O}_2$, as the micelles are distributed throughout the entire cluster of cells

Spheroids more accurately mimic the 3D structure, cell-cell interactions, and microenvironment of tissues *in vivo*. Therefore, we addressed the proof-of-concept for *in situ* detection of $^1\text{O}_2$ by using SOSG@Cy5-PIC/m in the spheroids of BxPC3 cells. In this experiment, oxaliplatin, which is a clinically approved drug that can induce $^1\text{O}_2$ by mitochondria damage [12], was used as a trigger for activating the SOSG signal in the micelles. Thus, free SOSG and SOSG@Cy5-PIC/m



157 were first incubated with the spheroid-cultured BxPC3 cells for 24 h.
 158 Then, oxaliplatin was administrated to the cells and incubated for 24 h.
 159 , 3-, 6- and 24-h to induce $^1\text{O}_2$ generation. The distribution of the
 160 micelles and the generation of $^1\text{O}_2$ inside the cells were imaged by
 161 CLSM. The SOSG signal from free SOSG and SOSG@Cy5-PIC/m was
 162 not observed in the cells exposed to oxaliplatin for 1 to 6 h (data not
 163 shown). However, the $^1\text{O}_2$ molecules produced after 24 h incubation
 164 with oxaliplatin were detectable by the SOSG in the SOSG@Cy5-
 165 PIC/m (Figure 4a). In contrast, the signal from free SOSG was
 166 undetectable. Previous studies have indicated that the access of
 167 SOSG into living mammalian cells presents major hurdles [25] and
 168 that SOSG is sensitive to extracellular $^1\text{O}_2$ molecules, which activates
 169 the probes before being internalized by the cells [27]. A comparison
 170 of the fluorescence intensity between free SOSG and SOSG@Cy5-
 171 PIC/m revealed a 15-fold increase in the SOSG signal intensity (Figure
 172 4b). The fluorescence intensities of the SOSG in SOSG@Cy5-PIC/m
 173 per spheroid were also evaluated by normalizing the SOSG signal
 174 with the Cy5 signal (Figure 4c). Compared to the spheroids treated
 175 with saline, the oxaliplatin-treated spheroids showed almost 2-fold
 176 higher SOSG/Cy5 ratio ($p < 0.05$). These results support the ability of
 177 SOSG@Cy5-PIC/m to detect $^1\text{O}_2$ in cellular systems. Given that ROS
 178 generation is commonly employed to induce cell death in cancer
 179 therapies, SOSG@Cy5-PIC/m offers a valuable tool for monitoring
 180 the therapeutic efficacy of such treatments. Additionally, the
 181 system's capability to encapsulate ROS-generating drugs, such as
 182 oxaliplatin used in this study, within its core enables a therapeutic
 183 approach that can simultaneously treat and track therapeutic efficacy
 184 with a single carrier. With further improvements and tuning, the
 185 SOSG@Cy5-PIC/m holds the potential of introducing a new paradigm
 186 in cancer theranostics, enabling the concurrent generation and
 187 detection of ROS.



188 **Figure 3.** (a) Time-lapse images of monolayer/spheroidal cultured BxPC3 cells
 189 with SOSG@Cy5-PIC/m observed by confocal laser-scanning microscopy
 190 (Blue: Nuclei [Ex/Emission (Em) = 405/446 nm], Red: SOSG@Cy5-PIC/m
 191 [Ex/Em = 633/661-750 nm]). (b) Time-dependent uptake of SOSG@Cy5-PIC/m
 192 for single cell/spheroid against monolayer/spheroidal cultured BxPC3 cells (n
 193 = 3), and all plots were statistically analysed by the Tukey-Kramer method (p
 194 < 0.05).

< 0.005). (c) Quantification of internalised SOSG@Cy5-PIC/m against BxPC-3
 spheroid. The relative intensity (RFU/pixel) is calculated from the pixel by
 pixel integration of the RFU on the white dotted line in Figure 3(a) (spheroid).

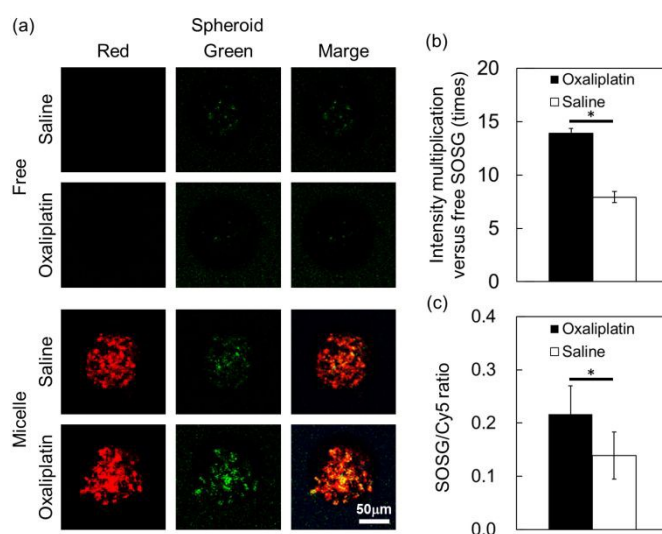


Figure 4. (a) Fluorescent imaging analysis of SOSG@Cy5-PIC/m against
 spheroidal cultured BxPC3 cells with oxaliplatin for 24 h co-incubation (Red:
 Cy5 [Ex/Em = 633/661-750 nm], Green: SOSG-EP [Ex/Em = 488/499-552 nm],
 yellow: colocalised micelles and SOSG). Scale bar: 50 μm. (b) Fluorescent
 intensity of oxaliplatin-stimulated SOSG in the micelles versus free SOSG with
 spheroidal culture (c) Fluorescent intensity ratio of SOSG/Cy5 in the
 spheroidal culture. The fluorescence intensity of SOSG/Cy5 per spheroid
 was calculated. Error bar means standard deviation ($n = 4$), and all plots were
 statistically analysed by the Student's t-test ($*p < 0.05$)

Conclusions

We successfully developed SOSG/Cy5-labeled PIC/m as probes for the detection of $^1\text{O}_2$ in biological environments. The SOSG@Cy5-PIC/m probes were internalised by BxPC3 pancreatic cancer cells in a time-dependent manner and were able to penetrate into the core of spheroidal cultures of BxPC3 cells. Thus, using these probes, we successfully detected the *in situ* $^1\text{O}_2$ generated by oxaliplatin in the spheroids. This method shows promise for the local analysis and quantification of $^1\text{O}_2$ in biological systems. The SOSG/Cy5-labeled PIC/m could be applied in a wide variety of treatments based on the oxidative responses, leading to an improved understanding of biological mechanisms, diagnostic tools, and therapeutic strategies.

Conflicts of interest

There are no conflicts to declare.

Acknowledgements

This work was supported by Grants-in-Aid for Scientific Research A (23H00546; H.C.), Grants-in-Aid for Exploratory Research (22K19541; H.C.), and the Fund for the Promotion of



- 228 Joint International Research (Fostering Joint International
229 Research (B), 21KK0197; H.C.), from the Japan Society for the
230 Promotion of Science (JSPS). This work was also partially
231 supported by the AMED Seeds A grant (23ym0126805j0001
232 H.C.).
- 233
- 234
- 235
- 236
- 237
238
239
240
241
242
243
244
245
246
247
248
249
250
251
252
253
254
255
256
257
258
259
260
261
262
263
264
265
266
267
268
269
270
271
272
273
274
275
276
277
278
279
280
281
282
283
284
285
286
- 25 A. Gollmer, J. Arnbjerg, F.H. Blaikie, B.W. Pedersen, T. Breitenbach, K. Daasbjerg, M. Glasius and P.R. Ogilby, *Photochem. Photobiol.*, 2011, **87**, 671-679.
- 26 H. Lin, Y. Shen, D. Chen, L. Lin, B.C. Wilson, B. Li and S. Xie, *J. Fluoresc.*, 2013, **23**, 41-47.
- 27 Y. Shen, H.Y. Lin, Z.F. Huang, D.F. Chen, B.H. Li and S. Xie, *Laser Phys. Lett.*, 2011, **8**, 232-238.

234 Data availability

235 A data availability statement (DAS) is submitted alongside.

236

237 References

- 238 1 T. Finkel and N.J. Holbrook, *Nature*, 2000, **408**, 239-247.
- 239 2 B. Halliwell and J.M. Gutteridge, *Free radicals in biology and medicine*, Oxford University Press, USA, 2015.
- 240 3 M. Schieber and N.S. Chandel, *Curr. Biol.*, 2014, **24**, R453-R462.
- 241 4 R. Scherz-Shouval and Z. Elazar, *Trends in Biochemical Sci.*, 2011, **36**, 30-38.
- 242 5 G. Lenaz, *IUBMB Life*, 2001, **52**, 159-164.
- 243 6 G. Kojda and D. Harrison, *Cardiovascular Res.*, 1999, **43**, 652-671.
- 244 7 G.-Y. Liou and P. Storz, *Free. Radic. Res.*, 2010, **44**, 479-496.
- 245 8 H. Yang, R.M. Villani, H. Wang, M.J. Simpson, M.S. Roberts, M. Tang and X. Liang, *J. Exp. Clin. Cancer Res.*, 2018, **37**, 266-266.
- 246 9 R.L. Berkow, D. Wang, J.W. Larrick, R.W. Dodson and T.H. Howard, *J. Immunol.*, 1987, **139**, 3783.
- 247 10 A. Ibrahim, S. Hirschfeld, M.H. Cohen, D.J. Griebel, G.A. Williams, R. Pazdur, *The Oncologist*, 2004, **9**, 8-12.
- 248 11 H. Zheng, W.H. Xiao and G. J. Bennett, *Experimental Neurology*, 2011, **232**, 154-161.
- 249 12 V. Santoro, R. Jia, H. Thompson, A. Nijhuis, R. Jeffery, K. Kiakos, A.R. Silver, J.A. Hartley and D.J. Hochhauser, *Natl. Cancer Inst.*, 2016, **108**, djv394.
- 250 13 N. M. Hasty and D.R. Kearns, *J. Am. Chem. Soc.*, 1973, **95**, 3380-3381.
- 251 14 M. Bobrowski, A. Liwo, S. Ołdziej, D. Jeziorek and T. Ossowski, *J. Am. Chem. Soc.*, 2000, **122**, 8112-8119.
- 252 15 A. Baker and J.R. Kanofsky, *Archives of Biochemistry and Biophysics*, 1991, **286**, 70-75.
- 253 16 J. Moan and E. Wold, *Nature*, 1979, **279**, 450-451.
- 254 17 A. Telfer, S.M. Bishop, D. Phillips, and J. Barber, *J. Biological Chem.*, 1994, **269**, 13244-13253.
- 255 18 C. Flors, M.J. Fryer, J. Waring, B. Reeder, U. Bechtold, P.M. Mullineaux, S. Nonell, M.T. Wilson and N.R Baker, *J. Experimental Botany*, 2006, **57**, 1725-1734.
- 256 19 A. Krasnovsky Jr, *Membrane Cell Biol.*, 1998, **12**, 665-690.
- 257 20 J. Baier, T. Fuß, C. Pöllmann, C. Wiesmann, K. Pindl, R. Engl, D. Baumer, M. Maier, M. Landthaler and W. Bäumlner, *J. Photochem. Photobiol. B: Biology*, 2007, **87**, 163-173.
- 258 21 H. Cabral, K. Miyata, K. Osada and K. Kataoka, *Chem. Rev.*, 2018, **118**, 6844-6892.
- 259 22 M.E. Davis, Z. Chen and D.M. Shin, *Nat. Rev. Drug Discov.*, 2008, **7**, 771-782.
- 260 23 A. Wibowo, K. Osada, H. Matsuda, Y. Anraku, H. Hirose, A. Kishimura and K. Kataoka, *Macromolecules*, 2014, **47**, 3086-3092.
- 261 24 Y. Anraku, H. Kuwahara, Y. Fukusato, A. Mizoguchi, T. Ishii, K. Nitta, Y. Matsumoto, K. Toh, K. Miyata, S. Uchida, K. Nishina, K. Osada, K. Itaka, N. Nishiyama, H. Mizusawa, T. Yamasoba, T. Yokota and K. Kataoka, *Nat. Commun.*, 2017, **8**, 1001.



Data availability statement

The authors confirm that the data supporting the findings of this study are available within the article. Raw data that support the findings of this study are available from the corresponding author, upon reasonable request.

